Atomistic Simulation Studies of Lithium and Proton Insertion in Spinel Lithium Manganates

Brett Ammundsen* and Jacques Rozière

Laboratoire des Agrégats Moléculaires et Matériaux Inorganiques ESA 5072, Université Montpellier 2, Place Eugène Bataillon, 34095 Montpellier Cédex 5, France

M. Saiful Islam

Department of Chemistry, University of Surrey, Guildford, Surrey GU2 5XH, U.K.

Received: April 25, 1997; In Final Form: July 23, 1997[⊗]

Atomistic simulation methods are used to investigate lithium and proton insertion in spinel lithium manganates. The energetics of lithium extraction and reinsertion by redox reactions in the $LiMn_2O_4$−λ-MnO_2 system are evaluated with respect to the formation of lithium vacancies or interstitials and to overall changes in lattice energy. Lithium migration mechanisms are also investigated, considering the energies for Li^+ ions to migrate through different pathways in the interstitial space of the lattice. The local structures around Mn 16d vacancies in spinels of composition $LiMn_2O_{4+\delta}$ and $Li_{1+x}Mn_{2-x}O_4$ are modeled to determine the effects of the vacancies on lithium and proton sites. Possible orientations of hydroxyl groups formed by inserted protons in the structure are examined, and a strong energetic preference for the hydroxyl groups to coordinate the 16d vacancies is found. A model is proposed for protonated spinel MnO_2 in which four hydroxyl groups are symmetrically distributed in planar configuration around each 16d vacancy.

Introduction

Insertion and extraction reactions of spinel manganese oxide with Li^+ have been extensively studied over the past 15 years.[1−27] From the electrochemical standpoint, spinel lithium manganates are strong candidates as alternative materials for secondary batteries.[1−14] Lithium may also be extracted from spinel lithium manganates by either chemical oxidation[15,16] or exchange with protons in aqueous solution.[17,18,21−25] The resulting delithiated spinel manganese oxides, called "λ-MnO_2", behave as sorbent materials with high selectivity for aqueous lithium ions.[18−22]

Mechanisms and sites of lithium extraction and insertion have been much discussed on the basis of experimental investigations. It is now well recognized that the chemical and electrochemical properties of spinel lithium manganates are very sensitive to the methods of preparation used, as the oxygen content can vary to give average manganese oxidation states between 3.5 and 4.0,[7,28] and up to a sixth of the manganese ions in $LiMn_2O_4$ can be substituted by lithium.[7] Crystallinity, ordering of lithium ions in the structure, and lithium−proton exchange capacity are all highly sensitive to these parameters.[5−8,14,21−25] However structure−property relationships have generally been discussed in terms of bulk structural and chemical properties, such as overall vacancy content, variations in the unit cell parameter, and average oxidation state. Only a few studies have attempted to understand the local structural perturbations resulting from manganese vacancies, lithium substitution for manganese, and proton insertion, and their effects on the properties of the materials.[14,23−25]

In this paper we examine specific problems relating to lithium extraction−insertion, proton insertion, and local order in spinel manganese oxide by the use of atomistic simulation techniques. Such techniques are well suited to probing polar inorganic solids at the atomic level and have been applied successfully to a rich variety of oxide systems, including studies of lithium insertion into Fe_3O_4 spinel[29,30] and protons in $LaMnO_3$ perovskites.[31,32] In the first stage of the present study, lithium extraction−insertion and lithium mobility are modeled in the $LiMn_2O_4$−λ-MnO_2 system, in which the $[Mn_2]O_4$ spinel framework is treated as a "perfect" lattice having no crystallographic defects. Then we examine the effects on the lattice structure and insertion properties when a fraction of the manganese in the $[Mn_2]O_4$ framework is absent or substituted by lithium, as occurs in spinel compounds of composition $LiMn_2O_{4+\delta}$ or $Li_{1+x}Mn_{2-x}O_4$. Finally, we consider the insertion of protons into the lattice by exchange with lithium, and model the positions of these protons in the local structure.

Atomistic Simulation Methods

The calculations in this work were performed using lattice energy minimization techniques embodied in the codes GULP[33] and CASCADE.[34] We present only the most relevant aspects of the techniques here, since they are described in greater detail elsewhere.[35]

The basis of the simulations is the specification of a potential model, which describes the energy of the system as a function of the atomic coordinates and allows the evaluation of the lattice energy. The Born model representation is commonly used for oxides, with the energy partitioned into long-range Coulombic interactions and short-range pair potentials. Polarization is treated using the "shell" model developed by Dick and Overhauser.[36] This model includes coupling between the short-range repulsive forces and ionic polarization and has been shown to simulate effectively both dielectric and elastic properties.

The calculations are based on well-established energy minimization procedures, with modeling of lattice defects performed using the two-region Mott−Littleton methodology.[37] An important feature of this method is the treatment of lattice relaxation around the defect or inserted ion which commonly causes perturbation of the surrounding lattice. The crystal lattice is simply divided into two concentric regions, so that ions in a

[⊗] Abstract published in *Advance ACS Abstracts,* September 15, 1997.

S1089-5647(97)01413-2 CCC: $14.00

spherical inner region (1) surrounding the defect are treated explicitly, while the ions in the remainder of the crystal are relaxed by quasi-continuum methods. In this way local relaxation is effectively modeled and the crystal is not considered simply a rigid lattice through which ion species diffuse. It is now well established that given reliable interatomic potentials and a sufficiently large inner region these simulation methods give accurate values of lattice polarization and Coulomb energies. For the calculations presented here, region 1 was defined so as to contain 250 atoms, which is expected to give reliable estimates of the energies of defect formation and migration, and allow local structural perturbations associated with the defect to be predicted.

The program GULP was used throughout most of the work presented here to calculate lattice energies and properties and minimum-energy lattice configurations, as well as energies associated with fully relaxed vacancy and interstitial defects. GULP furthermore allows fractional occupancies to be specified for crystallographic sites, implemented in the program through a mean field approach. This consisits of scaling interaction energies by the product of site occupancies. In the case of compounds containing manganese in a mixed oxidation state, this feature allows the simulation of homogeneous distributions of Mn^{3+} and Mn^{4+}. The use of the mean field approach involved an additional step in evaluating Mn^{3+}/Mn^{4+} oxidation energies, which should be mentioned. If, for example, we indicate by $Mn^{3.5+}$ the "mixed" Mn^{3+}/Mn^{4+} cation present at each 16d site in $LiMn_2O_4$, then the substitution of a Mn^{3+} ion in the lattice with a Mn^{4+} must be preceded by the substitution of a "mixed" $Mn^{3.5+}$ by a Mn^{3+}. The energy involved in this process is subtracted from that for the Mn^{4+} substitution to obtain the desired value. This approach has been applied recently to Ce^{3+}/Ce^{4+} redox processes in the CeO_2-ZrO_2 solid solution.[38]

Interatomic Potentials

The interatomic interactions within the lattice are described by ionic two-body potentials of the form

$$V_{ij}(r_{ij}) = [-Z_iZ_je^2/r] + [A_{ij}\exp(-r/\rho_{ij}) - C/r_{ij}^6] \quad (1)$$

where the first term represents the long-range Coulombic or electrostatic interaction between each pair of ions i and j in the structure, and the second term is an analytical function of the Buckingham form to describe electron charge cloud overlap repulsions and van der Waals forces. Ionic polarizability is incorporated by the shell model in which each ion is treated in terms of a core (representing the nucleus and core electrons) connected via a harmonic spring to a shell (representing the valence electrons).

The short-range potential parameters for each ion−ion interaction and shell model parameters used in this study are listed in Table 1. For $Mn^{3+}\cdots O^{2-}$ and $Mn^{4+}\cdots O^{2-}$ interactions, the parameters published in previous work[31,32,39] were refined to achieve an empirical fit to reported structural data for $LiMn_2O_4$ and λ-MnO_2.[8,40] In terms of the mean field approach for mixed-valent Mn in $Li_xMn_2O_4$, the short-range potential for the mixed species M can be expressed as:

$$V(M-O^{2-}) = x/2\ V(Mn^{3+}-O^{2-}) + (1 - x/2)\ V(Mn^{4+}-O^{2-}) \quad (2)$$

A potential model for the $Li^+\cdots O^{2-}$ interaction derived for Li_2O[41] was found to accurately reproduce experimental data for the local lattice structure around lithium in $LiMn_2O_4$ without need for further modification. We note that refinement of the harmonic force constant k for the O^{2-} ion was necessary to successfully reproduce structural data for lattice oxygen positions in the spinels. This allowed the ionic shell to shift 0.1−0.2 Å relative to the core atomic position, in the direction of the highly charged manganese ions which occupy three of the four lattice sites to which each oxygen is coordinated.

TABLE 1: Interatomic Potentials for the Lithium Manganates

Short-Range

interaction[a]	A (eV)	ρ (Å)	C (eV Å^6)
$Mn^{3+}\cdots O^{2-}$	1267.5	0.3231	0.0
$Mn^{4+}\cdots O^{2-}$	1345.15	0.3180	0.0
$Li^+\cdots O^{2-}$	426.48	0.3000	0.0
$O^{2-}\cdots O^{2-}$	22764.3	0.1490	43.0

Shell Model

species	Y (e)	k (eV Å^{-2})
Mn^{3+}	3.00	95.0
Mn^{4+}	4.00	95.0
Li^+	1.00	99999
O^{2-}	−2.24	9.85

[a] Potential cutoff = 12 Å.

TABLE 2: Calculated and Experimental[8,40] Crystal Properties for $LiMn_2O_4$ and λ-MnO_2

Unit Cell Parameters

	a_0 calc (Å)	a_0 expt (Å)
$LiMn_2O_4$	8.2407	8.2468
λ-MnO_2	8.0570	8.0445

Atomic Coordinates ($Fd3m$)

	species	x,y,z calc	x,y,z expt
$LiMn_2O_4$	Mn^{3+}, Mn^{4+} (16d)	0.5	0.5
	Li^+ (8a)	0.125	0.125
	O^{2-} (32e)	0.2623	0.2625
λ-MnO_2	Mn^{4+} (16d)	0.5	0.5
	O^{2-} (32e)	0.2633	0.2631

Interatomic Distances

		R calc (Å)	R expt (Å)
$LiMn_2O_4$	Mn−O	1.964	1.962
	Li−O	1.960	1.962
λ-MnO_2	Mn−O	1.913	1.912

Dielectric Constants and Lattice Energies

	ϵ^0_{11}	ϵ^∞_{11}	E_L (eV)
$LiMn_2O_4$	8.43	4.02	−214.94
λ-MnO_2	4.19	3.57	−251.42

Using the potentials of Table 1, the unit cell dimensions and ion positions were equilibrated under constant pressure conditions in simulations of "perfect" $LiMn_2O_4$ and λ-MnO_2 structures. The calculated lattice parameters, atomic coordinates and bond distances and their comparison with experimental values are listed in Table 2, showing a good agreement between experimental and simulated structures. We also give the dielectric constants and lattice energies calculated for the two crystals. We were unable to locate experimental dielectric data, but our models predict that the dielectric constants for these materials will be relatively low.

Inserted protons in the spinel manganese oxides are modeled as O−H groups located at oxygen sites in the lattice.[23,24] The O−H interaction is modeled using an attractive Morse potential

$$V(r) = D\{1 - \exp[-\beta(r - r_0)]\}^2 \quad (3)$$

TABLE 3: Potentials for the Proton Insertion Calculations

Parameters for the Morse Potential of the O−H Interaction

D (eV)	β (Å^{-1})	r (Å)
7.0525	2.1986	0.9845

Parameters for the Buckingham Potential Describing the Interaction between the Hydroxyl Proton and Lattice O^{2-}

A (eV)	ρ (Å)	C (eV Å^{-6})
311.97	0.35	0.0

the parameters for which were developed by Saul et al.[42] using ab initio quantum mechanical cluster calculations. These parameters are given in Table 3. Charges on the hydroxyl species were distributed across both ions to give an overall charge of −1 with O assigned −1.4263 and H +0.4263, which reproduces the correct dipole moment of the O−H group. The short-range interaction of the hydroxyl proton with other oxygen atoms in the lattice is described by a Buckingham potential having the parameters given in Table 3. We note that this modeling approach was recently used to investigate protons in perovskite-type oxides.[32]

Results and Discussion

1. The $LiMn_2O_4$−λ-MnO_2 System. *Lithium Extraction and Insertion.* A schematic representation of the spinel structure of $LiMn_2O_4$ is shown in Figure 1. The structure can be described in the *Fd*3*m* space group as a cubic close-packed array of oxygens in the 32e position. Half the octahedral interstices, at the 16d position, are occupied by the manganese ions, forming a three-dimensional framework of edge-sharing [MnO_6] octahedra. Lithium ions occupy one-eighth of the tetrahedral interstices, at the 8a position. Each 8a tetrahedron shares common faces with four neighboring empty octahedra at the 16c position which, together with 48f tetrahedra, form a three-dimensional network of interstitial space through which lithium ions may diffuse.

Lithium extraction from $LiMn_2O_4$ is achieved either electrochemically, for example during the charging cycle in lithium batteries, or chemically by reaction in aqueous acid or with an oxidizing agent. The extraction involves overall oxidation of the manganese oxide, so that completely delithiated λ-MnO_2 would contain manganese in a predominantly tetravalent state. The reaction is topotactic, the $[Mn_2]O_4$ sublattice of the spinel structure remaining intact. Reported experimental data show that the extraction proceeds in three steps.[22] For $1 < x < 0.5$ in $Li_xMn_2O_4$, the reaction is observed to be single phase with a continuous decrease of the unit cell parameter from 8.25 to ∼8.13 Å. When x falls below 0.5, a second spinel phase having a unit cell parameter of ∼8.04 Å appears, which corresponds to quasi-delithiated λ-MnO_2. The quantity of λ-MnO_2 phase then increases as x decreases, and the 8.13 Å phase progressively disappears.

Lithium reinsertion into λ-MnO_2 occurs during discharge of the lithium cell, and also takes place when λ-MnO_2 is immersed in aqueous solutions of lithium in the presence of hydroxide ions.[19] Up to the composition $LiMn_2O_4$, lithium is reinserted into the 8a tetrahedral sites of the spinel, accompanied by reduction of 1 equiv of lattice Mn(IV) to Mn(III). A similar three-step process occurs as in extraction, with replacement of the 8.04 Å λ-MnO_2 phase by a ∼8.13 Å phase in the compositional range $0.16 > x > 0.44$, followed by a continuous increase in the unit cell parameter up to the 8.25 Å $LiMn_2O_4$ phase.[19,22]

To better understand the energetics of lithium extraction and insertion by redox reactions in these materials, it is useful to consider (i) the energy to remove a lithium ion from its tetrahedral 8a site in $LiMn_2O_4$, (ii) the energy to bring a lithium ion onto a vacant 8a site in λ-MnO_2, and (iii) the lattice relaxation energy associated with oxidation or reduction of a localized manganese ion. These values relate to "isolated" energies with zero reference at infinity and can be combined in full redox processes. The relevant values have been calculated and are reported in Table 4. We have also calculated the energies for the pair clusters [Mn^{4+}/Li^+ vacancy] and [Mn^{3+}/Li^+ interstitial] for $LiMn_2O_4$ and λ-MnO_2, respectively. The significance of such localized pairs is indicated by the binding energy, calculated as the difference between the energy of the clustered species and those of the isolated components.

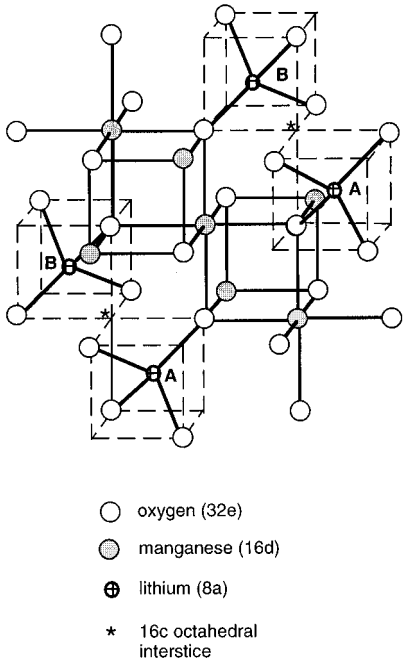

Figure 1. Schematic representation of the spinel structure of $LiMn_2O_4$. Lithium ions in different 8a sublattices are identified as A and B.

TABLE 4: Energies (eV) of Defect Species in $LiMn_2O_4$ and λ-MnO_2

	Li vacancy (8a)	Mn(III) → Mn(IV) (16d)	8a−16d cluster pair	binding energy for cluster pair[a]
$LiMn_2O_4$	9.23	−40.79	−31.91	−0.35
	Li^+ interstitial (8a)	Mn(IV) → Mn(III) (16d)	8a−16d cluster pair	binding energy for cluster pair[a]
λ-MnO_2	−7.86	41.31	32.53	−0.92

[a] With respect to isolated 8a and 16d defects, our sign convention is such that a negative value indicates that the cluster is bound.

Comparison of the energies reported in Table 4 and the lattice energies given in Table 2 allows predictions to be made for lithium extraction in the $LiMn_2O_4$−λ-MnO_2 system which correlate well with experimental observations. The difference between the lattice energies (ΔE_L) of $LiMn_2O_4$ and λ-MnO_2 is 36.48 eV. This is ca. 4.5 eV greater in magnitude than the total energy calculated for the formation of an isolated 8a vacancy and the oxidation of an isolated Mn^{3+} ion to Mn^{4+} in $LiMn_2O_4$. This suggests an energetic preference for complete extraction of lithium and formation of the manganese(IV) oxide with long-range order over isolated defect formation. The favorable binding energy of −0.35 eV found for the localized [Mn^{4+}/Li^+ vacancy] pair indicates that the presence of these species in neighboring sites will lead to a greater lowering of

TABLE 5: Binding Energies of Li^+ 8a Clusters in λ-MnO_2

		binding energy (eV per Li)[a]
neighboring 8a sites	2 Li^+	0.37
	3 Li^+	0.69
next-neighboring 8a sites	2 Li^+	0.31
	3 Li^+	0.60

[a] With respect to isolated Li^+ interstitials (8a).

the lattice energy than when the species are isolated from each other in the crystal.

In the inverse process of lithium reinsertion, the total energy calculated for an isolated 8a Li^+ interstitial and the reduction of a Mn(IV) species to Mn(III) in λ-MnO_2 is ca. 4 eV lower than ΔE_L. This suggests the presence of unfavorable Coulombic interactions with increasing lithium content. It is noteworthy that the binding energy of -0.90 eV for the localized [Mn^{3+}/Li^+ interstitial] pair is highly favorable. This suggests that the reduction of Mn(IV) to Mn(III) will favor lithium insertion at a neighboring 8a tetrahedral site.

Structural studies have shown that the partially lithiated 8.13 Å phase observed for $x = 0.5$ in $Li_xMn_2O_4$ is characterized by the ordering of lithium ions on only one of two sublattices into which the 8a sites can be divided.[19] These two sublattices are identified as A and B in Figure 1. The ordering on one sublattice, which maximizes Li−Li distances in the crystal, is attributed to interactions between neighboring lithium ions and between lithium ions and the host manganese oxide lattice.[12] To examine the influence of Li−Li interactions, we calculated binding energies for λ-MnO_2 when neighboring and near-neighboring 8a sites are filled with two or three lithium ions. The results, given in Table 5, show large positive increases in binding energy as the number of neighboring lithium ions increases. These results indicate that Li clusters of this type would be unfavorable without the corresponding charge compensation. Nevertheless, the calculated energies in Table 5 are consistent with experimental observations in showing that, when lithium clusters begin to form in the spinel manganese oxide, a favorable lowering of energy will be achieved by adopting ordered arrangements in which Li−Li Coulombic interactions are minimized.

From the calculated lattice energies for $LiMn_2O_4$ and λ-MnO_2, it is possible to estimate an energy of lithium insertion. For example, for the simple reaction

$$\mathrm{Li(s)} + 2\lambda\text{-}\mathrm{MnO_2(s)} \rightarrow \mathrm{LiMn_2O_4(s)} \qquad (4)$$

the energy of insertion may be estimated as

$$\Delta E_{\mathrm{insertion}} = \Delta E_L - I(\mathrm{Mn^{III}}) + E_S(\mathrm{Li}) + I(\mathrm{Li}) \qquad (5)$$

where ΔE_L is the overall lattice energy change associated with the insertion, $I(Mn^{III})$ is the fourth ionization energy of manganese (51.2 eV), E_S(Li) is the enthalpy of sublimation of lithium (1.65 eV), and I(Li) is the first ionization energy of lithium (5.39 eV). Using the absolute lattice energy difference between λ-MnO_2 and $LiMn_2O_4$ (Table 2), such a calculation gives a value $\Delta E_{\mathrm{insertion}} = -7.68$ eV, which indicates that lithum insertion in λ-MnO_2 with regard to solid lithium is a highly favorable process. This is in qualitative accord with observation, although we find a discrepancy in quantitative terms with an experimental enthalpy value of ca. 4 eV for electrochemical insertion using lithium metal as the anode.[10] The discrepancy will be partly due to the uncertainty in the ionization energy for manganese which is derived from gas-phase measurements. Ideally we would use an ionization term derived within the lithium manganate crystal field. This warrants further investigation, perhaps by quantum mechanical methods. We note, nevertheless, that according to the above equation it is the favorable reduction of Mn(IV) which energetically drives the reaction against an unfavorable change in lattice energy. This is consistent with the view that the presence of easily reducible cations facilitates the insertion of lithium into spinel oxides.

TABLE 6: Energies of Isolated Li^+ Interstitials in λ-MnO_2

site	E (eV)
8a tetrahedral	−7.86
16c octahedral	−6.76
48f tetrahedral	−3.12
8b tetrahedral	10.49

Lithium Sites and Migration. Lithium extraction and insertion in spinel manganese oxide require diffusion of the Li^+ ions through the interstitial space of the lattice. We consider here the mobility of lithium ions in λ-MnO_2 and $LiMn_2O_4$. In the case of an isolated lithium ion diffusing through otherwise delithiated λ-MnO_2, the energy barriers to migration will be determined by the relative energies of the sites encountered as the ion hops through the interstitial channels. The energies for a lithium interstitial at the unoccupied tetrahedral and octahedral interstices in λ-MnO_2 have been calculated and are given in Table 6. The relative magnitudes show that the 8a tetrahedral site is most favorable for Li^+ in λ-MnO_2, agreeing with experimental data which show insertion of lithium into this site for $0 < x < 1$ in $Li_xMn_2O_4$.[3] Lithium occupation of the 16c octahedral sites in λ-MnO_2 is less favorable than that of the 8a by 1.1 eV. The 48f and 8b tetrahedral sites are energetically unfavorable for Li^+ ions as they share two and four faces, respectively, with Mn 16d octahedra.

Migration pathways in λ-MnO_2 will therefore be restricted to the three-dimensional network of interstitial space defined by 8a and 16c sites. Within the spinel structure the 8a tetrahedra and 16c octahedra share faces, providing continuous migration pathways through the lattice. By calculating the energy change for small displacements of the lithium ion, the energy profiles of possible paths have been calculated. The lowest energy path for a Li^+ ion to move between two neighboring 8a sites is found to be that passing in a linear path parallel to a [111] direction through a 16c site. The 16c site represents a saddle point, and therefore the activation energy for 8a → 8a migration is the 1.1 eV required to pass through this site.

Lithium diffusion coefficients for $Li_xMn_2O_4$ compositions $0 < x < 1$ have been experimentally determined in the range 10^{-11}−10^{-10} $cm^2\ s^{-1}$ in aqueous systems[27] and 10^{-11}−10^{-8} $cm^2\ s^{-1}$ in nonaqueous systems.[5,9,12,13] The observed variations are probably related both to the different experimental methods used and to small but significant differences in sample composition and morphology. Evaluation of the data indicates that lithium ion diffusion in spinel manganese oxide is rather slow compared with layered-structure materials, although one of the cited studies[27] estimates an activation energy of ca. 0.5 eV. However, for intermediate $Li_xMn_2O_4$ compositions, the changes in energy which occur during lithium migration will be modified by mutual interactions between lithium ions and by changes in the manganese oxidation state. In particular, experimental data shows that lithium ordering on the 8a sublattices has a strong effect on lithium diffusion.[12,13]

To evaluate the energetics of lithium mobility in $Li_xMn_2O_4$ materials in which 8a sites are more fully occupied, it is pertinent to consider the kinds of disordered structures which might be present. Diffusion will be controlled primarily by the energy parameters associated with the formation and migration of point defects. We have therefore calculated energies for the formation of isolated vacancies and interstitials in $LiMn_2O_4$ and report

TABLE 7: Isolated Defect Energies in $LiMn_2O_4$

defect	E (eV)
Li 8a vacancy	9.23
Li interstitial in 16c	−5.93
Mn 16d vacancy	69.66
Mn interstitial in 16c	−57.13
O 32e vacancy	25.40
O interstitial in 16c	−12.02

TABLE 8: Formation Energies of Frenkel and Schottky Defects in $LiMn_2O_4$

defect[a]	E (eV per defect)
Li Frenkel	1.65
Mn Frenkel	6.27
O Frenkel	6.69
Schottky	5.03

[a] Frenkel = vacancy + interstitial; Schottky = cation vacancies + anion vacancies + E_L.

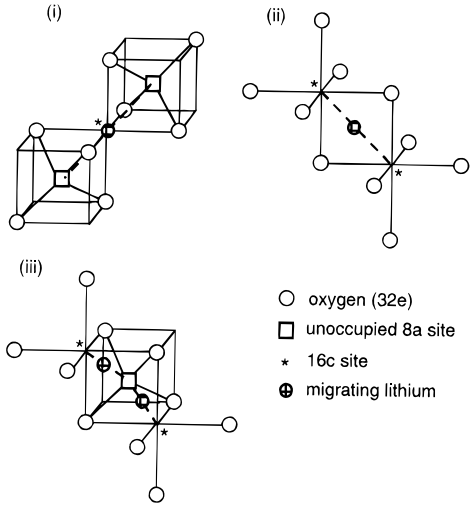

Figure 2. Lithium diffusion mechanisms in $LiMn_2O_4$ containing 8a vacancies or 16c lithium interstitials: (i) vacancy jump, (ii) interstitial jump, (iii) "interstialcy" jump.

these in Table 7. The values are then combined to give the energies of formation of Frenkel and Schottky defects in Table 8. These calculations suggest that the predominant mode of intrinsic disorder in $LiMn_2O_4$ is of the lithium Frenkel type. The energy per defect, 1.65 eV, indicates that a small concentration of thermally generated lithium interstitial and vacancy disorder will be present in the pure material even at ambient temperatures. Li (8a) vacancies and interstitials in $LiMn_2O_4$ will of course also result from lithium extraction and insertion, respectively.

Activation energies for Li^+ migration in $LiMn_2O_4$ were then calculated considering three mechanisms: (i) migration by an 8a vacancy jump, for which the saddle point has the migrating lithium ion in the intermediate 16c interstice, (ii) a direct interstitial jump between neighboring 16c sites through a shared edge, and (iii) a concerted "interstitialcy" jump, involving the correlated motion of lithium ion pairs in which the migrating interstitial lithium ion displaces an 8a lithium into a neighboring 16c site. The three mechanisms are schematically represented in Figure 2, and the calculated activation energies are given in Table 9. The 0.84 eV for a vacancy jump in $LiMn_2O_4$ is lower than the value calculated for lithium hopping through the 16c site in λ-MnO_2. This mechanism is expected to dominate in $Li_xMn_2O_4$ materials for $x < 1$. It is interesting to find that a low-energy pathway for lithium diffusion is present between 16c interstices. The interstitial jump therefore presents an alternative pathway in the presence of intrinsic Frenkel disorder

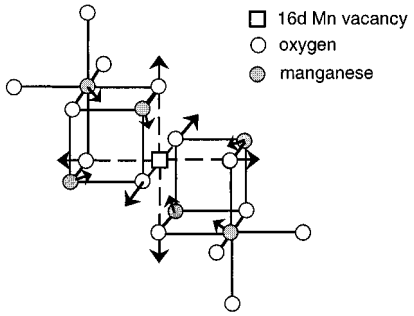

Figure 3. Oxygen and manganese displacements surrounding a 16d vacancy in $LiMn_2O_{4+\delta}$.

TABLE 9: Activation Energies for Lithium Ion Migration in $LiMn_2O_4$

mechanism	E (eV)
vacancy	0.84
interstitial	0.60
interstitialcy	1.25

and may become increasingly important as lithium appears in 16c sites during electrochemical insertion in $LiMn_2O_4$.

2. Mn (16d) Vacancies in $LiMn_2O_{4+\delta}$ and $Li_{1+x}Mn_{2-x}O_4$. There has been much recent interest in spinel lithium manganates having a manganese average oxidation state greater than 3.5, as this modifies the lithium insertion properties.[6,7,22−25,43−45] Such spinels occur when the preparation conditions favor the incorporation of "excess" oxygen to give compositions $LiMn_2O_{4+\delta}$, $0 < \delta < 0.5$, or by raising the Li/Mn ratio to give compositions $Li_{1+x}Mn_{2-x}O_4$, $0 < x < 0.33$. In the case of $LiMn_2O_{4+\delta}$ materials, the excess oxygen gives rise to cation vacancies, predominantly on 16d sites but also on 8a sites.[6] The precise stoichiometry of such materials is, however, difficult to control synthetically. In the case of stoichiometric $Li_{1+x}Mn_{2-x}O_4$ compositions, as the excess lithium x increases from 0 to 0.33 it is incorporated into the spinel with a corresponding increase in the manganese oxidation state according to the formula $Li_{1+x}Mn^{3+}{}_{1-3x}Mn^{4+}{}_{1+2x}O_4$. The increased oxygen/manganese stoichiometry resulting from the higher manganese oxidation state in this case also gives rise to manganese "vacancies" on the 16d sites. Neutron diffraction studies have indicated that these 16d sites are occupied by the excess lithium,[8] although at least one report has suggested that lithium associated with the 16d defect may be disordered with some lithium appearing in 16c sites.[46]

To model the local structure around Mn 16d vacancies in lithium manganates, the minimum energy configurations were calculated for materials having one 16d vacancy per unit cell, with a compensating increase in overall manganese oxidation state. This produces a unit cell of composition $Li_8Mn_{15}O_{32}$, corresponding to a value of $\delta = 0.12$ in $LiMn_2O_{4+\delta}$ and an average manganese oxidation state of 3.73. The relaxed lattice configuration around the vacancy is schematically represented in Figure 3. The six oxygens coordinated to the vacant octahedral site relax away from the vacancy center with a displacement of ∼0.16 Å from their perfect lattice positions, whereas manganese ions in neighboring 16d sites are displaced toward the vacancy center by ∼0.1 Å. It has recently been suggested that, in the presence of such manganese vacancies, lithium ions in neighboring 8a sites are partially "pinned" due to the excess negative charge on the oxygen ions coordinating the vacancy.[14] We have therefore calculated energies for lithium vacancies on 8a sites both neighboring and isolated from the Mn 16d vacancy. The values, given in Table 10, indicate that a lithium ion neighboring the vacancy requires 0.6 eV greater

TABLE 10: Energies for Lithium 8a Vacancies in the $LiMn_2O_{4.12}$ Lattice

lithium site	energy (eV)
8a isolated from Mn (16d) vacancy	7.04
8a neighboring Mn (16d) vacancy	7.63

TABLE 11: Energies for Lithium Configurations around a 16d Vacancy in $LiMn_2O_4$ into Which an "Excess" Lithium Ion Has Been Introduced

configuration of Li positions[a]	E (eV)
(i) 6(8a) + (16d)	−9.77
(ii) 6(8a) + (16c)	−7.44
(iii) 6(16c) + (16d)	−2.90

[a] See text.

energy to be removed from its 8a site, consistent with this "pinning" effect.

To investigate the local structure of the $Li_{1+x}Mn_{2-x}O_4$ system, an "excess" interstitial lithium ion was introduced into the $LiMn_2O_4$ lattice in the presence of a 16d manganese vacancy. The relative energies for three different lithium configurations around the vacancy were then calculated: (i) the excess lithium ion in the 16d vacancy and other lithium ions remaining in 8a sites; (ii) the excess lithium ion in a 16c interstice neighboring the vacancy and other lithium ions in 8a sites; (iii) the excess lithium ion in the 16d vacancy, but the six neighboring lithium ions displaced into 16c interstices. The energies, given in Table 11, predict that the most stable configuration is that in which the excess lithium occupies the 16d vacancy with the other lithium ions remaining in their characteristic 8a sites. This agrees with the long-range structure determined from neutron diffraction data by Thackeray et al.[8]

3. Proton Insertion in λ-MnO_2. The increased manganese oxidation state in compounds of composition $LiMn_2O_{4+\delta}$ and $Li_{1+x}Mn_{2-x}O_4$ limits the quantity of lithium that can be extracted by oxidation of the host matrix. In aqueous acid, however, the lithium ions in Mn(IV)-rich spinels are readily exchanged for protons without modification of the manganese oxidation state nor of the long-range spinel framework structure.[22−25] The delithiated spinels can be modeled as λ-MnO_2 with Mn vacancies at 16d sites, overall charge neutrality being maintained by the inserted protons.

Vibrational data from infrared and inelastic neutron scattering spectroscopies indicate that the inserted protons in λ-MnO_2 form hydroxyl groups by bonding to lattice oxygen ions.[23,24] Orientations of the hydroxyl hydrogen toward nearest-neighbor oxygens at different O···O distances in the perfect lattice structure have previously been considered.[23] The local environment of a proton bonded to oxygen in the perfect λ-MnO_2 lattice is schematically represented in Figure 4a. If the 16d sites are fully occupied by manganese, all oxygen atoms are on equivalent 32e sites. Nearest-neighbor oxygens are at (i) 2.55, (ii) 2.85, and (iii) 3.14 Å and can be considered as possible sites for hydrogen bonding. We have calculated here the energies for orientation of the hydroxyl proton along each of these O···O axes, replacing a lattice O^{2-} with a OH^-, fixing the proton position at the minimum-energy O−H distance in each case (0.93−0.98 Å), and allowing the surrounding lattice to fully relax. The calculated energies, given in Table 12, confirm that orientation of the hydroxyl group along either axis (i) or (ii) is energetically unfavorable due to the proximity of 16d manganese ions. Orientation of the hydrogen along axis (iii) toward neighboring oxygen at 3.14 Å is found to be the most favorable of the three positions, in agreement with the previously described model from spectroscopic studies.[23] In this position the hydroxyl group is orientated along one of three identical edges of the 8a tetrahedron. For this model, we have also calculated the energy allowing the OH group to fully relax, which is included in Table 12.

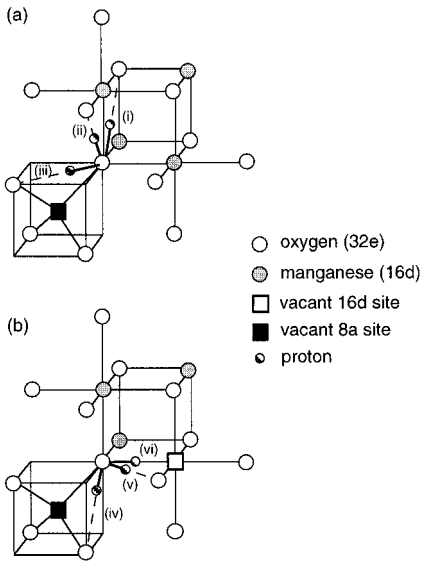

Figure 4. (a) Fixed orientations of the O−H group for which energies have been calculated in the λ-MnO_2 perfect lattice and (b) additional orientations calculated with a Mn 16d vacancy.

TABLE 12: Energies for OH^- on an O^{2-} Site in the "Perfect" λ-MnO_2 Lattice, Calculated for Different O−H Orientations

orientation[a]	E (eV)
(i)	21.67
(ii)	16.29
(iii)	12.86 (12.09[b])

[a] Shown in Figure 4a. [b] Allowing full relaxation of O−H.

TABLE 13: Energies for OH^- on an O^{2-} Site Adjacent to a Mn 16d Vacancy in the λ-MnO_2 Lattice, Calculated for Different O−H Orientations

orientation[a]	E (eV)[b]
(i)	15.76
(ii)	10.61
(iii)	7.67
(iv)	6.58 (6.55[c])
(v)	7.41
(vi)	8.58

[a] Shown in Figure 4a,b. [b] Energy of formation of the 16d vacancy has been subtracted. [c] Allowing full relaxation of O−H.

Calculations were then performed with a Mn vacancy introduced at one of the three 16d sites to which the hydroxyl oxygen is coordinated. The vacancy changes the symmetry of the oxygen site and also results in local structural perturbations, so that the O···O axes are no longer equivalent. After recalculating energies for OH with the proton positions of Figure 4a, we have also calculated energies for three additional orientations in the proximity of the 16d vacancy center, shown in Figure 4b. Position (iv) differs from the type (iii) positions in being orientated closer to the 16d vacancy. Position (v) lies on an octahedral edge shared between the vacant 16d site and the 16c interstitial site. Position (vi) was calculated with the hydroxyl proton orientated directly toward the vacant 16d center. The energies, reported in Table 13, are lower than those calculated when the hydroxyl is coordinated to three 16d sites occupied by manganese (Table 12). This suggests an energetic preference for formation of the hydroxyl at an oxygen site coordinating a 16d vacancy. The lowest energy orientation corresponds to the (iv) position along the 8a tetrahedral edge

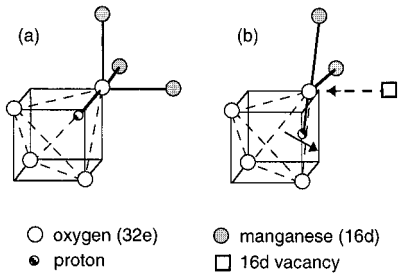

Figure 5. Orientations of the fully relaxed lattice hydroxyl group in (a) the λ-MnO_2 perfect lattice and (b) coordinating a Mn 16d vacancy.

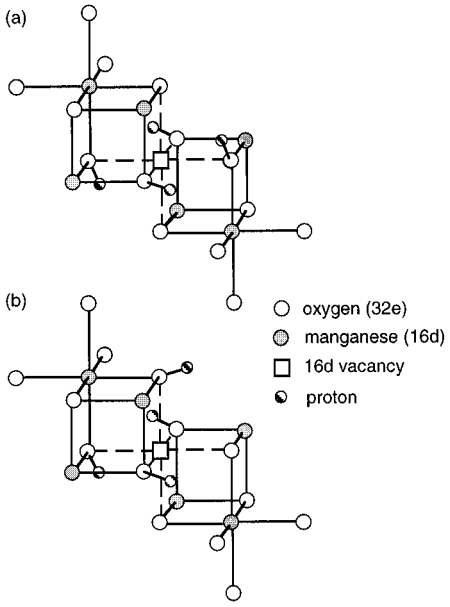

Figure 6. Configurations for four charge-compensating hydroxyl groups at a Mn 16d vacancy.

closest to the Mn 16d vacancy. It is worth noting that despite the absence of a cation, orientation of the proton into the vacant 16d site involves an unfavorable increase of ca. 2 eV relative to the (iv) position.

The local structural effect of the Mn 16d vacancy on the orientation of the O−H group is illustrated in Figure 5. When the hydroxyl is positioned at a lattice oxygen site in the perfect λ-MnO_2 lattice, the fully relaxed position is orientated toward the center of the 8a tetrahedron, with an O−H distance of 0.98 Å. This orientation places the proton equidistant from the three oxygens defining the opposite corners of the 8a tetrahedron. Therefore this may be considered an average of three equivalent type (iii) positions in which the hydroxyl group might form a hydrogen bond to one of these oxygens. However when the hydroxyl is positioned at a 16d vacancy, the minimum-energy configuration changes. All oxygens coordinating the vacancy, including the hydroxyl oxygen, relax outward from the vacancy center by ~0.3 Å along the normal octahedral axes. The hydroxyl proton now prefers an orientation toward that edge of the 8a tetrahedron which is orientated closest to the vacant 16d site. In this configuration, the hydroxyl group is preferentially orientated toward only one of the three oxygens (Figure 5b).

Charge compensation requires that four protons should be inserted for each 16d Mn vacancy in λ-MnO_2. Lowest-energy configurations were therefore calculated for clusters of four hydroxyl groups arranged around a 16d vacancy as illustrated in Figure 6a,b. The energies calculated for these clusters are reported in Table 14. The cluster represented in Figure 6a, where all four hydroxyl groups are symmetrically positioned in planar configuration at corners of the vacant 16d octahedron,

TABLE 14: Energies for Configurations of Four Hydroxyl Groups on Lattice O^{2-} Sites around a 16d Vacancy in λ-MnO_2

configuration[a]	E (eV)[b]
symmetric (planar)	32.28
asymmetric	33.54
next-nearest oxygens	46.87

[a] Shown in Figure 6. [b] Energy of formation of the 16d vacancy has been subtracted.

is more stable by 1.26 eV than the alternative nonsymmetric configuration illustrated in Figure 6b. It is important to note that the clusters in which the four hydroxyls are directly located at the 16d vacancy were calculated to be much more stable than any arrangement in which the hydroxyls are located away from the vacancy. An example is given in Table 14 for a cluster in which the four hydroxyl ions are located at the next-nearest oxygen positions to the 16d vacancy. The unfavorable increase in energy in this case is ca. 15 eV. We therefore predict that exchange of lattice lithium for charge-compensating protons in Mn(IV)-rich materials will only occur with formation of hydroxyl groups at 16d vacancies. If the vacancies are randomly distributed in the crystal, these hydroxyl groups will be located in approximately identical local environments and each will adopt the same characteristic orientation with respect to the 16d vacancy center as that illustrated in Figure 5b. This is in agreement with the vibrational spectra of proton-exchanged λ-MnO_2 compounds which show a single hydroxyl deformation mode, from which it is concluded that the majority of inserted protons are located in identical sites.[23] It is interesting to note that the formation of a "nest" of four hydroxyl groups to compensate a tetravalent cation vacancy is known in garnets and other silicates and has been modeled atomistically.[47,48]

Conclusions

The present study demonstrates how atomistic simulation techniques can be used to examine lithium and proton insertion processes in spinel manganese oxides. Our discussion has drawn attention to the following key aspects of lithium and proton insertion.

(1) The important energetic factor contributing to topotactic extraction of lithium from $LiMn_2O_4$ is a favorable lowering of lattice energy in the formation of the delithiated λ-MnO_2 phase. On the other hand, lithium reinsertion is driven by the ease of reduction of Mn^{4+}, although unfavorable Coulombic interactions as the lattice lithium content increases will raise the energy required for insertion. This is in agreement with experimental observations that as x in $Li_xMn_2O_4$ approaches 1, the voltage level of lithium batteries drops, and that lithium reinsertion in hydroxide solutions occurs with increasing difficulty.

(2) The lithium ion preferentially occupies the 8a tetrahedral site on insertion into λ-MnO_2 in accordance with observation. Lithium diffusion through the three-dimensional network will be dependent on the energy required to pass over 16c octahedral sites, which represent saddle points in the migration pathways between 8a sites.

(3) Manganese 16d vacancies will change the site energies for neighboring 8a lithium ions in agreement with experimental data that suggest that these lithiums are "pinned" by such vacancies. In compounds of composition $Li_{1+x}Mn_{2-x}O_4$, the "excess" x lithium prefers to be located in the 16d site unoccupied by manganese rather than in a 16c interstice.

(4) A large energetic preference is found for hydroxyl groups in protonated λ-MnO_2 to coordinate to manganese vacancies rather than to form at other oxygen sites in the lattice. The

orientation of the O−H group will be affected by the local structural and electronic perturbations due to the vacancy. Our calculations predict that the lowest energy position for the hydroxyl proton is along that O···O axis defining the edge of the 8a tetrahedron most closely orientated toward the vacant 16d site.

The calculations described here represent the first detailed application of atomistic simulation techniques to the study of lithium and proton species in manganese oxide, but there remain important problems to be investigated. In particular the modeling of proton insertion, transfer, and migration in the spinel manganese oxide system requires further work. A mechanism for the formation of lattice water needs to be elucidated as this has also been observed in protonated λ-MnO_2 and appears to have an important structural role.[23] An investigation is planned combining the present approach with quantum mechanical calculations to consider proton migration. Such studies have already been successfully carried out for perovskite structures,[32] and extension to spinel systems should greatly enhance our understanding of proton transport phenomena in metal oxides in general.

Acknowledgment. The authors thank M. Sakib Khan and Mark Read for useful aid in running GULP and CASCADE. B.A. thanks the British Council for a travel grant to perform work at Surrey University.

References and Notes

(1) Thackeray, M. M.; David, W. I. F.; Bruce, P. G.; Goodenough, J. B. *Mater. Res. Bull.* **1983**, *18*, 461.
(2) Thackeray, M. M.; Johnson, P. J.; de Picciotto, L. A.; Bruce, P. G.; Goodenough, J. B. *Mater. Res. Bull.* **1984**, *19*, 179.
(3) David, W. I. F.; Thackeray, M. M.; de Picciotto, L. A.; Goodenough, J. B. *J. Solid State Chem.* **1987**, *67*, 316.
(4) Ohzuku, T.; Kitagawa, M.; Hirai, T. *J. Electrochem. Soc.* **1990**, *137*, 769.
(5) Guyomard, D.; Tarascon, J. M. *J. Electrochem. Soc.* **1992**, *139*, 937.
(6) de Kock, A.; Rossouw, M. H.; de Picciotto, L. A.; Thackeray, M. M.; David, W. I. F.; Ibberson, R. M. *Mater. Res. Bull.* **1990**, *25*, 657.
(7) Thackeray, M. M.; de Kock, A.; Rossouw, M. H.; Liles, D. C.; Bittihn, R.; Hoge, D. *J. Electrochem. Soc.* **1992**, *139*, 363.
(8) Thackeray, M. M.; de Kock, A.; David, W. I. F. *Mater. Res. Bull.* **1993**, *28*, 1041.
(9) Pistoia, G.; Wang, G.; Wang, C. *Solid State Ionics* **1992**, *58*, 285.
(10) Bach, S.; Pereira-Ramos, J. P.; Baffier, N.; Messina, R. *Electrochim. Acta* **1992**, *37*, 1301.
(11) Barker, J.; Pynenburg, R.; Koksbang, R. *J. Power Sources* **1994**, *52*, 185.
(12) Barker, J.; West, K.; Saïdi, Y.; Pynenburg, R.; Zachau-Christiansen, B.; Koksbang, R. *J. Power Sources* **1995**, *54*, 475.
(13) Saïdi, M. Y.; Barker, J.; Koksbang, R. *J. Solid State Chem.* **1996**, *122*, 195.
(14) Gao, Y.; Reimers, J. N.; Dahn, J. R. *Phys. Rev. B* **1996**, *54*, 3878.
(15) Hunter, J. C. *J. Solid State Chem.* **1981**, *39*, 142.
(16) Mosbah, A.; Verbaère, A.; Tournoux, M. *Mater. Res. Bull.* **1983**, *18*, 1375.
(17) Shen, X.-M.; Clearfield, A. J. *J. Solid State Chem.* **1986**, *64*, 270.
(18) Leont′eva, G. V.; Chirkova, L. G. *Zh. Prikl. Khim.* **1988**, *61*, 734.
(19) Ooi, K.; Miyai, Y.; Katoh, S.; Maeda, H.; Abe, M. *Langmuir* **1989**, *5*, 150.
(20) Ooi, K.; Miyai, Y.; Katoh, S.; Maeda, H.; Abe, M. *Langmuir* **1990**, *6*, 289.
(21) Ooi, K.; Miyai, Y.; Sakakihara, J. *Langmuir* **1991**, *7*, 1167.
(22) Feng, Q.; Kanoh, H.; Miyai, Y.; Ooi, K. *Langmuir* **1992**, *8*, 1861.
(23) Ammundsen, B.; Burns, G. R.; Jones, D. J.; Rozière, J. *Chem. Mater.* **1995**, *7*, 2151.
(24) Ammundsen, B.; Aitchison, P. B.; Burns, G. R.; Jones, D. J.; Rozière, J. *Solid State Ionics* **1997**, *97*, 269.
(25) Ammundsen, B.; Burns, G. R.; Jones, D. J.; Rozière, J. *Chem. Mater.* **1996**, *8*, 2799.
(26) Kanoh, H.; Feng, Q.; Miyai, Y.; Ooi, K. *J. Electrochem Soc.* **1993**, *140*, 3162.
(27) Kanoh, H.; Feng, Q.; Miyai, Y.; Ooi, K. *J. Electrochem Soc.* **1995**, *142*, 702.
(28) Le Cras, F.; Strobel, P.; Anne, M.; Bloch, D.; Soupart, J.-P.; Rousche, J.-C. *Eur. J. Solid State Inorg. Chem.* **1996**, *33*, 67.
(29) Islam, M. S.; Catlow, C. R. A. *J. Solid State Chem.* **1988**, *77*, 180.
(30) Islam, M. S. *Philos. Mag. A* **1993**, *68*, 667.
(31) Cherry, M.; Islam, M. S.; Catlow, C. R. A. *J. Solid State Chem.* **1995**, *118*, 125.
(32) (a) Cherry, M.; Islam, M. S.; Gale, J. D.; Catlow, C. R. A. *J. Phys. Chem.* **1995**, *99*, 14614. (b) Islam, M. S.; Cherry, M. *Solid State Ionics* **1997**, *97*, 33.
(33) (a) Gale, J. D. GULP (General Utility Lattice Program); Royal Institution of GB and Imperial College: London, 1991−1996. (b) Gale, J. D. *J. Chem. Soc., Faraday Trans.* **1997**, *93*, 629.
(34) Leslie, M. Report DL/SCI/TM31T; EPSRC Daresbury Lab, 1982.
(35) Catlow, C. R. A. In *Solid State Chemistry Techniques*; Cheetham A. K.; Day, P., Eds.; Clarendon Press: Oxford, 1987; Chapter 7.
(36) Dick, B. G.; Overhauser, A. W. *Phys. Rev.* **1958**, *112*, 90.
(37) Mott, N. F.; Littleton, M. J. *Trans. Faraday Soc.* **1938**, *34*, 485.
(38) Balducci, G.; Kaspar, J.; Fornasiero, P.; Graziani, M.; Islam, M. S.; Gale, J. D. *J. Phys. Chem. B* **1997**, *101*, 1750.
(39) Lewis, G. V.; Catlow, C. R. A. *J. Phys. C* **1985**, *18*, 1149.
(40) Fong, C.; Kennedy, B. J.; Elcombe, M. M. *Z. Kristallogr.* **1994**, *209*, 941.
(41) Bush, T. S.; Gale, J. D.; Catlow, C. R. A.; Battle, P. D. *J. Mater. Chem.* **1994**, *4*, 831.
(42) Saul, P.; Catlow, C. R. A.; Kendrick, J. *Philos. Mag. B* **1985**, *51*, 107.
(43) Rossouw, M. H.; de Kock, A.; de Picciotto, L. A.; Thackeray, M. M.; David, W. I. F.; Ibberson, R. M. *Mater. Res. Bull.* **1990**, *25*, 173.
(44) Tarascon, J. M.; McKinnon, W. R.; Coowar, F.; Bowmer, T. N.; Amatucci, G.; Guyomard, D. *J. Electrochem. Soc.* **1994**, *141*, 1421.
(45) Gummow, R. J.; de Kock, A.; Thackeray, M. M. *Solid State Ionics* **1994**, *69*, 59.
(46) Berg, H.; Bergstrom, O.; Gustafsson, T.; Kelder, E.; Thomas, J. O. Eighth International Meeting on Li Batteries, Osaka, Japan, 1996; p 26.
(47) Cohen-Addad, C.; Ducros, P.; Bertaut, E. F. *Acta Crystallogr.* **1967**, *23*, 220.
(48) Wright, K.; Freer, R.; Catlow, C. R. A. *Phys. Chem. Miner.* **1994**, *20*, 500.